Mathematical Biosciences and Engineering

http://www.aimspress.com/journal/MBE

Mathematical Biosciences and Engineering, 5(x): xxx–xxx
DOI:
Received: xx 2019
Accepted: xx 2019
Published: xx 2019

Type of article

Estimation of Vital Parameters of Glioblastoma Multiforme Growth Dynamics from a Model with Explicit Birth and Death Rates

Lifeng Han[1], Steffen Eikenberry[1], Changhan He[1], Lauren Johnson[1], Mark Preul[2], Eric Kostelich [1], and Yang Kuang[1,*]

[1] School of Mathematical and Statistical Sciences, Arizona State University, Tempe, AZ 85287, USA

[2] Department of Neurosurgery Research, Barrow Neurological Institute, St. Josephs Hospital and Medical Center, Phoenix, AZ 85013, USA

* **Correspondence:** kuang@asu.edu

Abstract: Glioblastoma multiforme (GBM) is an aggressive brain cancer with grim prognosis. Its morphology is characterized by layered structure, i.e., an inner necrotic core and an outer rim of proliferating cells. This structure can be observed in magnetic resonance images. A mathematical model of GBM growth with explicit birth and death rate is proposed. This model generates a traveling wave which mimic the cancer progression. We develop some novel methods to approximate key characteristics of the wave profile, which can be compared with image data. Several simplistic forms of growth and death terms and their parameter identifiability are studied. We use image data of GBM patients to get personalized parameterization of the model, of which the biological and clinical implications are discussed.

Keywords: Glioblastoma multiforme modeling; parameter estimation; traveling wave; necrosis; proliferation

1. Introduction

Glioblastoma multiforme (GBM) is a type of the most aggressive brain cancer. Patients with GBM have a mean survival length less than 15 months from the time of diagnosis [15]. Its fast progression is characterized by highly proliferating and invasive cancer cells. The information on individual GBM patients are very scarce while challenges to treat GBM are numerous. A key piece of information clinical doctors may have for their GBM patients are MRI images. Often there is only one image that lead to the diagnosis and the patients are immediately scheduled for surgery. The main questions for surgeons are how much and where to cut and how soon the cancer will emerge and where. These are decades old questions that surface in other type of cancer treatments.

GBM morphology manifests a layered structure: there is a necrotic core at the center, a band of proliferating cells at the outer rim and a transition layer of quiescent cancer cells in between. GBM can be visualized by magnetic resonance (MR) imaging, which is commonly used to inform clinical decisions. One of the hallmarks of cancer in general, and GBM in particular, is its heterogeneity between individual patients. This heterogeneity imposes a challenge to GBM treatment.

Appropriate mathematical models may offer a way to tackle this challenge. Mathematical modeling has already provided many valuable insights to our understanding of cancer and its treatment [10]. Mathematical models on GBM are formulated to provide new tools for studying the growth of gliomas and for practical applications (see [12] for a review). A popular type of those models oftem takes the form of a system of reaction-diffusion equations. In many cases [6, 5, 20], those systems generate a traveling wave solution of which the speed is of great interests since it is related to how fast cancer progresses.

However, models which confront the heterogeneity of GBM directly by utilizing spatiotemporal patient-specific data are rare. Swanson and her collaborators [22, 14, 7] is one of the few teams which focus on this endeavor. They employed variants of the well-known Fisher's equation to study cancer cells' proliferation (P) and invasion (I) dynamics [4] (hence called PI model in [7]) and parameterized it using patient MR images. The estimated proliferation and diffusion parameters and a model-derived metric called days gained are deemed to be instrumental to clinical treatments.

Treating the cancer cells as a single species can be a gross simplification and by doing so the structured morphology of GBM is lost. Although there are modeling efforts taking into account of multi-species nature of cancer cells [3, 21], they are usually too complicated to be practically useful given scarcity of patient specific images.

For most GBM patients and their doctors, available MRI images maybe all taken at the same day or at just two different days. Practical modeling efforts must be constrained by such brutal data limitation and formulate models which can be parameterized with the images at hand. Recognizing this reality, we propose a model which includes two species of cancer cells, i.e., proliferating and quiescent, and is capable of exploiting the structural information offered by only one or two MRI images.

Gliomas can only be imaged indirectly on MRI, and are typically characterized, on T1-weighted sequences, by a large, often necrotic core region surrounded by a bright enhancing rim that correlates with high blood vessel density and (presumably) rapid cell proliferation. This core and rim is usually surrounded by a large expanse of edema that is visible on T2-weighted MRI, and may represent diffusely invasive, highly motile GBM cells. Thus, we have three digital marks from imaging: necrotic radius, enhancing radius, and T2 (or maximum) radius. We hypothesize that a relatively simple mathematical model framework may capture all these three digital marks, and yield insights into the relative contributions of cellular proliferation, motility, and necrosis to the observed image features.

The paper is organized as following. We first describe our model and its assumptions. Then we demonstrate that the model has a traveling wave solution and present the approximate wave profile. We devise a simple procedure to estimate patient-specific parameters by fitting the approximate wave profile to that of patient images. Identifiability of parameters is also discussed. Moreover, we apply this parameter estimation procedure to obtain the cancer vital dynamics parameters (consisting of the rate of cancer cell proliferation, death and diffusion) for several patients.

2. Model and method

2.1. Model description

To model the growth of GBM, we propose a system of reaction-diffusion equations

$$\frac{\partial p}{\partial t} = \nabla \cdot \left[\frac{Dp}{p+q} \nabla (p+q) \right] + \tilde{g}(w)p - \tilde{\delta}(w)p, \tag{2.1a}$$

$$\frac{\partial q}{\partial t} = \nabla \cdot \left[\frac{Dq}{p+q} \nabla (p+q) \right] + \tilde{\delta}(w)p, \tag{2.1b}$$

where two species are considered: proliferating cells and quiescent cells whose density at time t and location x is represented by $p(x,t)$ and $q(x,t)$ respectively. We assume the flux of total population due to migration is $-D\nabla(p+q)$ where D is a constant diffusion coefficient. It is further assumed that the proportion of the total flux contributed by each species equals their proportion of the total population. This diffusion term is believed to be a realistic account of cancer cell movements [18].

Per capita birth rate is $\tilde{g}(w)$ and the proliferating cells become quiescent with per capita rate $\tilde{\delta}(w)$. Both of them are functions of w. We define $w = 1 - p - q$, interpreted as availability of space or some generic nutrient (we call it growth factor henceforth). By doing so, we have scaled the maximum cell density to be 1. In our model, necrosis is not explicitly included but can be regarded as being lumped into q. This choice is supported by the fact that MR only visualizes proliferating cells and does not distinguish between quiescence and necrosis. Our motivation of keeping the model simple enough is to estimate model parameters based on information that can be provided by the images. Note that quiescent cells can not become proliferating again but only turns into necrosis. Therefore $\tilde{\delta}(w)$ can be viewed as death rate.

In order to make the model biologically reasonable, we impose the following constraints on $g(w)$ and $\delta(w)$:

$$\tilde{g}'(w) \geq 0, \tilde{\delta}'(w) \leq 0, \tilde{g}(1) \geq \tilde{\delta}(1) = 0, \tilde{\delta}(0) > \tilde{g}(0) = 0. \tag{2.2}$$

That is, birth/death should increase/decrease with availability of the growth factor, and there is more birth than death at maximum growth factor while there is only death and no growth in absence of growth factor. It is also assumed that death rate is negligible at maximum growth factor. With these assumptions, it can be shown that the solution of (2.1) stay nonnegtive and is bounded by $p+q \leq 1$ for all t with the usual suitable initial condition.

We can only estimate up to three parameters based on the three pieces of information we can derive from MR images. Therefore we want a few more restrictions on $\tilde{g}(w)$ and $\tilde{\delta}(w)$ for the ease of parameter estimation and ensure their identifiability. Since we can only introduce two more parameters in addition to diffusion coefficient D, we introduce ρ and k into $\tilde{g}(w)$ and $\tilde{\delta}(w)$ respectively and indicate their dependence on the parameters as $\tilde{g}(w;\rho)$ and $\tilde{\delta}(w;k)$. It is desirable to make the proliferating rate at maximum growth factor be ρ and death rate at zero growth factor be k, i.e., $\tilde{g}(1,\rho) = \rho$, $\tilde{\delta}(0;k) = k$. For reasons that will become clear later, we pick the functional form which can be written as $\tilde{g}(w;\rho) = \rho g(w)$ and $\tilde{\delta}(w;k) = k\delta(w)$. Some examples of $g(w)$ and $\delta(w)$ include the cumulative distribution function of beta distribution family (see left pane of Figure 3). Although we have stated several additional assumptions, it should be noted that they impose little impact on the generality and flexibility of our model. The benefit of including them will become clear in the section of parameter estimation.

2.2. Approximate wave profile

In most biological applications of reaction-diffusion models, solutions quickly take the forms of traveling waves. MRI images of GBM cancer growth suggests we can approximate the cancer population growth curve by a traveling wave solution of its growth model. In order to uniquely identify and accurately approximate GBM growth model parameters, it is highly desirable to obtain some analytic approximation of the travel wave so a computational match of the image wave profile and the approximate model wave profile can be made. To this end and for simplicity, we consider one spatial dimension. It is justified by the fact that the tumor is mostly spherical and at the time of diagnosis its radius is large enough so that radial effect is negligible. Together with the aforementioned assumptions, the equations may take the following forms:

$$\frac{\partial p}{\partial t} = \frac{\partial}{\partial x}\left[\frac{Dp}{p+q}\frac{\partial}{\partial x}(p+q)\right] + \rho g(w)p - k\delta(w)p, \tag{2.3a}$$

$$\frac{\partial q}{\partial t} = \frac{\partial}{\partial x}\left[\frac{Dq}{p+q}\frac{\partial}{\partial x}(p+q)\right] + k\delta(w)p. \tag{2.3b}$$

We nondimensionlize the system using the characteristic length $\sqrt{D/k}$ and the characteristic time $1/k$ so that $x = \sqrt{D/k}\hat{x}$ and $t = \hat{t}/k$, which leads to

$$\frac{\partial p}{\partial \hat{t}} = \frac{\partial}{\partial \hat{x}}\left[\frac{p}{p+q}\frac{\partial}{\partial \hat{x}}(p+q)\right] + \hat{\rho} g(w)p - \delta(w)p, \tag{2.4a}$$

$$\frac{\partial q}{\partial \hat{t}} = \frac{\partial}{\partial \hat{x}}\left[\frac{q}{p+q}\frac{\partial}{\partial \hat{x}}(p+q)\right] + \delta(w)p, \tag{2.4b}$$

where $\hat{\rho} = \rho/k$. We are seeking a traveling wave solution, i.e., $p(\xi) = p(\hat{x} - c\hat{t}), q(\xi) = q(\hat{x} - c\hat{t})$ where c is wave speed. Substituting these into (2.4) gives

$$(\frac{p}{p+q}(p+q)')' + cp' + \hat{\rho} g(w)p - \delta(w)p = 0, \tag{2.5a}$$

$$(\frac{q}{p+q}(p+q)')' + cq' + \delta(w)p = 0, \tag{2.5b}$$

where the prime indicates the derivative with respect to ξ. Linearizing at the wave head, i.e., substitute an ansztz $p = Ae^{-r\xi}$ and $q = Be^{-r\xi}$ into (2.5) gives $(r^2 - cr + \rho)A = 0$. For biologically realistic wave front, we expect $A > 0$, $B > 0$ and $r > 0$. This requires that $c^2 > 4\rho$, which implies that the minimum speed of the wave $c_{\min} = 2\sqrt{\hat{\rho}}$. It is numerically verified that the minimum speed is exactly the asymptotic speed, i.e., $c = c_{\min}$.

To obtain a approximate wave profile, we adopt a popular method first used by Canosa in [1]. We rescale the wave coordinate $z = -\xi/c$, which leads to

$$\frac{1}{c^2}(\frac{p}{p+q}(p+q)')' - p' + \hat{\rho} g(w)p - \delta(w)p = 0, \tag{2.6a}$$

$$\frac{1}{c^2}(\frac{q}{p+q}(p+q)')' - q' + \delta(w)p = 0, \tag{2.6b}$$

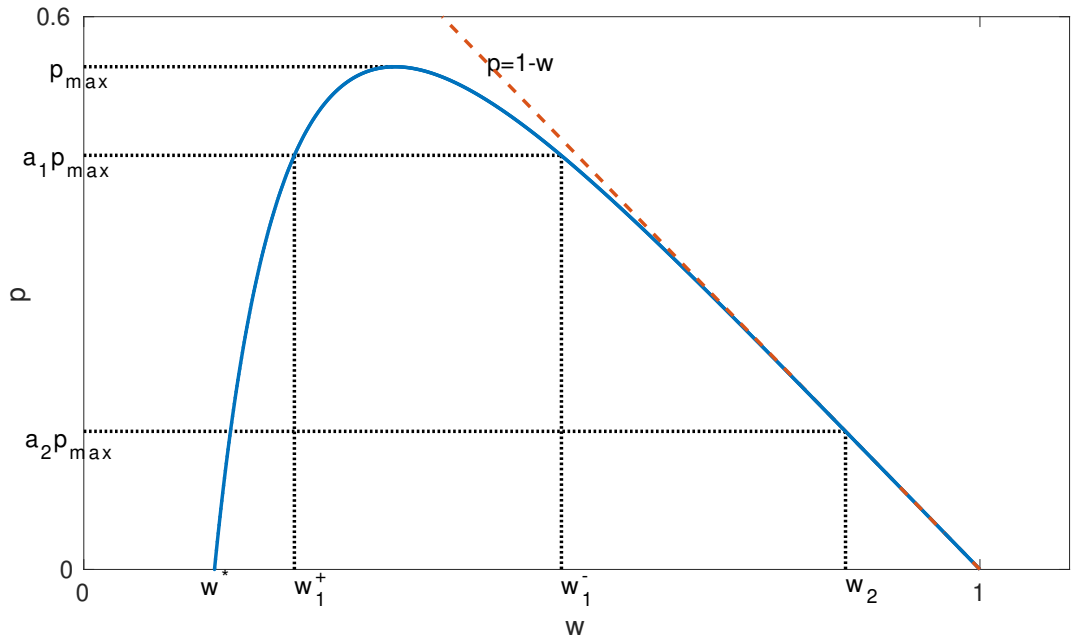

Figure 1. A typical trajectory that connects (0,1) and $(0, w^*)$ in the phase plane. Given $\delta(w)$ and $g(w)$, this trajectory can be found by integrating (2.8). This trajectory represents an approximate traveling wave solution and its existence under general assumptions is shown in supplemental material.

where the prime indicates the derivative with respect to z. Assuming that $1/c^2$ is small, we neglect the first terms of (2.6a),(2.6b). Writing the system in terms of p and w, we obtain the following reduced system

$$\frac{dw}{dz} = -\hat{\rho} p g(w), \tag{2.7a}$$

$$\frac{dp}{dz} = p(\hat{\rho} g(w) - \delta(w)), \tag{2.7b}$$

which is amenable to phase plane analysis. The approximate wave solution corresponds to a trajectory that leaves $(0, 1)$ and ends at $(0, w^*)$ with $w^* \in [0, 1)$ (see Figure 1). Its existence based on assumptions (2.2) is shown in the appendix. Dividing (2.7b) by (2.7a) yields

$$\frac{dp}{dw} = \frac{\delta(w)}{\hat{\rho} g(w)} - 1. \tag{2.8}$$

Upon integration we get p as a function of w, i.e., $p = p(w)$, which we will make use of in the next section.

2.3. Parameter estimation

We first discuss the three key values which we may obtain from MR images and use that to fit our model. There are two types of MR: T1 highlights high density of proliferating cells while T2

has a lower detection threshold. We denote their detection thresholds as $100 \times a_1\%$ and $100 \times a_2\%$ of $p_{\max} = \max_z\{p(z)\}$ (the actual maximum density of proliferating cells given by the traveling wave solution) with $a_1 > a_2$. To fit our 1-D model, we convert necrotic core volume, T1 volume and T2 volume into equivalent spheres with their radius denoted by R_0, R_1 and R_2, respectively (to do: figure needed). Therefore, the width of proliferating rim denoted as L_1 and L_2 for T1 and T2 images can be calculated, i.e., $L_1 = R_1 - R_0$ and $L_2 = R_2 - R_1$. Typically, there are two MR scans before surgery: one is at diagnosis and the other is right before surgery with a usual time interval of a few weeks [22]. The image-derived wave velocity V is the change in tumor radius divided by the length of this time interval.

From our approximate wave profile, we can compute the corresponding quantities to match with images (Figure 2). The rim width (in dimensional form) is computed as below

$$\ell_1 = \frac{\sqrt{D\rho}}{k} \int_{w_1^-}^{w_1^+} \frac{dz}{dw} dw, \tag{2.9a}$$

$$\ell_2 = \frac{\sqrt{D\rho}}{k} \int_{w_1^+}^{w_2} \frac{dz}{dw} dw, \tag{2.9b}$$

where $w_1^{\pm}$ and w_2 satisfy $p(w_1^{\pm}) = a_1 p_{\max}, p(w_2) = a_2 p_{\max}$ with $p(w)$ resulted from integration of (2.8). Additionally, model-derived wave speed $c = 2\sqrt{\rho D}$ can be matched with image-derived speed V. Thus we have three nonlinear equations

$$\{\ell_1 = L_1, \ell_2 = L_2, c = V\}, \tag{2.10}$$

from which we hope to find parameters D, ρ and k. Due to the assumptions we made before, we can simply take the ratio of (2.9a) and (2.9b), which gives

$$f(\hat{\rho}) \equiv \frac{\int_{w_1^-}^{w_1^+} \frac{dz}{dw} dw}{\int_{w_1^-}^{w_1^+} \frac{dz}{dw} dw} = \frac{L_1}{L_2}, \tag{2.11}$$

where we note that the integrals are a function of $\hat{\rho}$. (2.11) can be solved for $\hat{\rho}$ analytically in special cases or numerically in general. We note that the monotonicity of $f(\cdot)$ is important for identifiability of parameters. Once we find $\hat{\rho}$, i.e., the ratio ρ/k, all parameters can be found by back substitution.

The above method requires two MR scans taken at two consecutive times before surgery in order to obtain image-derived wave speed. If the second image is not available, another approximation can be made to rescue this situation. Generally, tumor age can be estimated by the tumor radius divided by the wave speed. However, age estimation differs in terms of which radius (say R_1 or R_2) to use. This discrepancy can be explained by the common observation that tumor grows exponentially at the initial stage and then linearly later on [10]. This initial exponential growth stage needs to be taken into account as a correction to the aforementioned tumor age estimation. The initial exponential growth stage potentially affects the age estimation using R_2 more than the one using R_3. Assuming that from $t = 0$ to $t = t^*$, the T1 volume of the tumor expands exponentially and then follows linear growth with speed $2\sqrt{\rho D}$, and that exponential growth stage of T2 volume is negligible, we have

$$\frac{R_1 - r_0(e^{\rho t^*})^{1/3}}{2\sqrt{\rho D}} + t^* = \frac{R_2}{2\sqrt{\rho D}}, \tag{2.12}$$

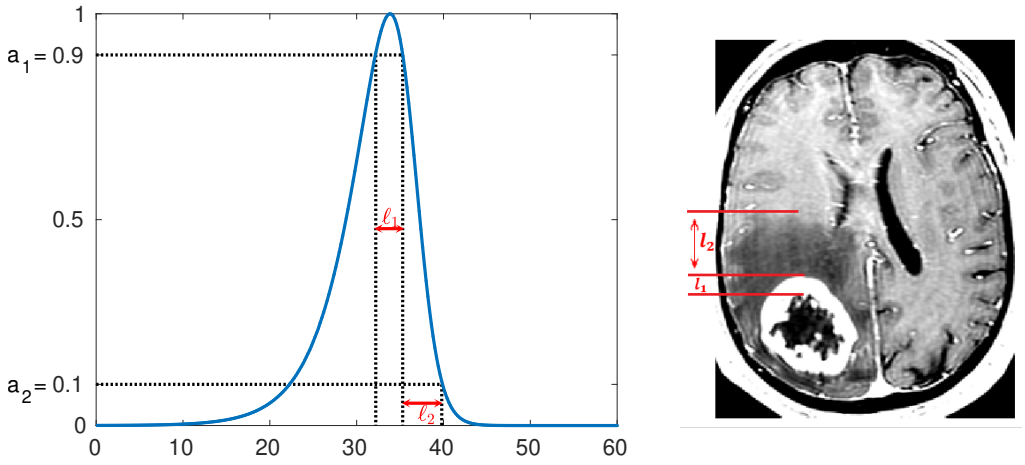

Figure 2. Left: normalized wave profile generated by the model. Right: tumor profile seen in MR image. Parameter estimation is done by matching model-derived quantities, e.g., ℓ_1 and ℓ_2, to the corresponding image-derived ones.

by equating the two age estimations. Coming from the assumption of exponential growth of tumor volume, the term $r_0(e^{\rho t^*})^{1/3}$ is the T1 radius at the end of the exponential growth stage, where r_0 is the initial tumor radius . Replacing the last equation in (2.10) with the equation above, we have again three equations for which we can solve for the three unknown parameters.

3. Results

We first investigate the monotonicity of $f(\cdot)$ for some specific choice of $g(w)$ and $\delta(w)$ because it is crucial for parameter identifiability. Given our restrictions (2.2) on $g(w)$ and $\delta(w)$, the cumulative distribution function of Beta distribution family suits our purposes. Therefore, we let $g(w) = B(w;\alpha_g,\beta_g)$ and $\delta(w) = 1 - B(w;\alpha_\delta,\beta_\delta$, where $B(w;\alpha,\beta)$ is the cdf of Beta distribution with shape parameters α and β. By tweeting α and β, we can get linear, sigmoid and concave up/down curves (see left pane of Figure 3). It turns out that our framework is very robust to those choices, i.e., monotonicity of $f(\cdot)$ is well preserved (right pane of Figure 3). As we can see, choosing $g(w) = B(w;2,2)$ and $\delta(w) = B(w;1,3)$ gives larger range of $f(\cdot)$ and thus more flexibility in parameter estimation. Moreover, the sigmoid curves given by this choice are believed to be biologically relevant (most enzymatic reaction rates have the same shape with respect to reactant concentration). Therefore, we focus on this choice and move on to find patient specific parameters using their MR images.

We parameterize our model with patient's data in which there is only one MR scan before surgery. In Table 1 we summarize the image-derived tumor radii and the corresponding parameters estimated by the method introduced in the previous section. We observe substantial variation of the parameters among individual patients.

We compare our approximate quantities to those obtained from the numerical solution of the model. As shown in Figure 4, the approximated results match with numerical results well except for some discrepancy for L_2 when $\hat{\rho}$ is small. It is not a surprise since the approximation is based on assumption

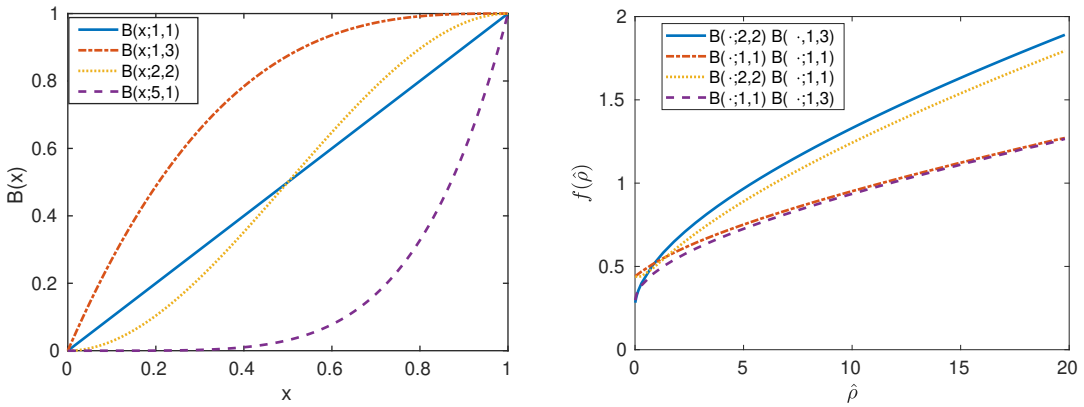

Figure 3. Left: cdf of some beta distribution. These functions satisfy (2.2) and serve as reasonable candidates to phenomenologically represent biological response to limitation of growth factors. Right: monotonicity of $f(\cdot)$ given different choices of $g(w)$ and $\delta(w)$ as indicated in the legend. All choices lead to monotonic function $f(\cdot)$ and hence identifiable parameters.

of large $c = 2\sqrt{\hat{\rho}}$. Moreover, numerical approximation of L_2 is prone to errors due to the fixed grid size and large rate of change around the threshold of L_2. Overall, we are convinced that our approximation is accurate for the parameter range arisen from the image data.

Table 1. Radii of equivalent tumor sphere derived from T1 and T2 images and the corresponding vital parameters estimated by our protocol. We have preset $a_1 = 0.9, a_2 = 0.1$, $r_0 = 0.21$ mm and $t^* = 30$ days, which are adapted from numbers found in the literature [22, 19], and based on experimentally verifiable hypotheses.

Patient no.	R_0, mm	R_1, mm	R_2, mm	D, mm^2 day^{-1}	ρ, day^{-1}	k, day^{-1}
1	14.87	15.24	15.83	0.2873	0.0529	0.0152
2	20.73	22.87	20.35	0.9009	0.0462	0.0623
3	27.77	26.96	19.83	0.108	0.0568	0.0107
4	20.48	37.03	23.8	0.6747	0.0445	0.1342
5	26.34	8.17	38.05	0.7374	0.0476	0.0426
6	38.24	14.2	13.31	0.1057	0.0635	0.0041
7	10.91	8.29	34.33	1.2655	0.046	0.0645

4. Discussion

The diffusion term in (2.3) falls into a general category called cross diffusion [11], a phenomenon in which the gradient in the concentration of one species can cause a flux of another species. This type of cross diffusion considered here was studied in a more general and theoretical context [17]. In [18], the authors justified the adoption of this proportion-based cross diffusion in a tumor growth model by recognizing that tumor cell migration is "contact inhibited", i.e., the presence of one type

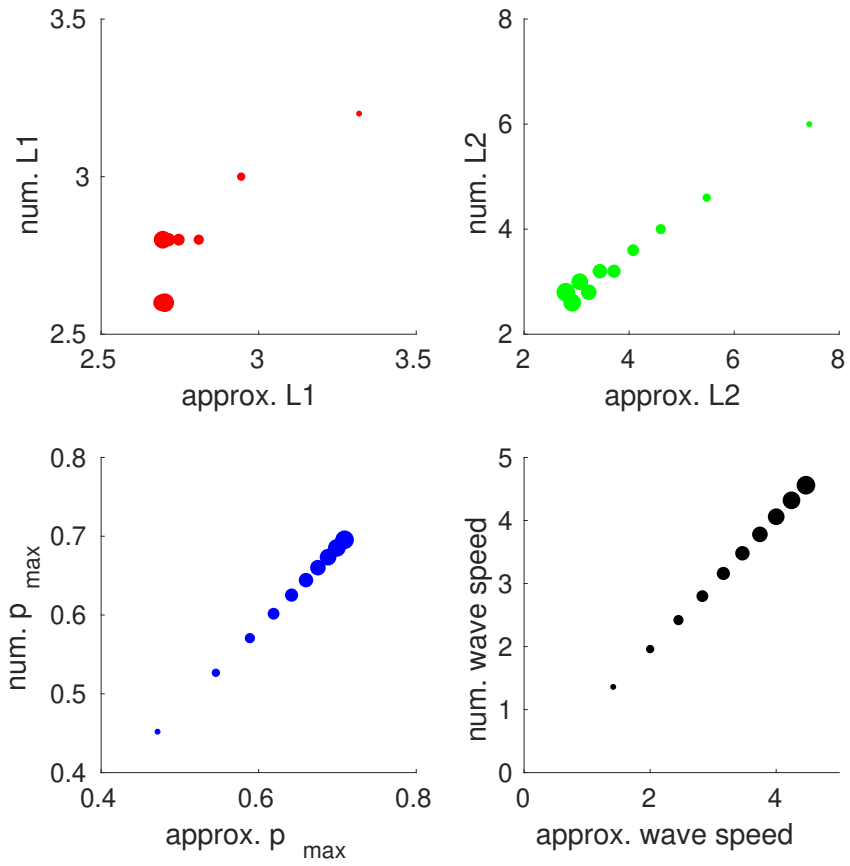

Figure 4. Scatter plots of approximate wave profile characteristics (on horizontal axis) verses the ones obtained by numerical simulation (on vertical axis) for a range of $\hat{\rho}$ from 0.5 to 5 by incremental 0.5. The size the the dot corresponds to the value of $\hat{\rho}$. The dots scatter closely to the diagonal line with slope 1, indicating agreement between the numerical solution and our approximation.

of cell prevents the movements of the other. In other words, the movements of one type of cell drags along other type of cells with it. It is believed that this type of diffusion is more realistic than simple linear diffusion (Fickian) in a sense that it prevents unrealistic mixing of cells. Other types of density-dependent diffusion are considered in modeling GBM migration [19]. Although a more complete picture of cell migration needs to include mechanisms such as chemotaxis and haptotaxis, tumor growth is oftentimes seen as diffusive and a careful choice of diffusion term is believed to be sufficient to model cell migration in many cases. Although the most accurate form of diffusion is debatable in the context of GBM, we note that in our analysis the exact form of diffusion does not matter since the second derivatives are dropped in (2.6). The diffusion coefficient does play an important role in the linearized wave head where it affects the wave speed, and in characteristic length where its square root scales the space. Whereas the scale invariant part of the wave profile is mostly determined by the exact form of birth and death for which we did a thorough exploration. So we believe that our model should capture the essence of the tumor morphology revealed by MR images.

Traveling wave solution is not uncommon in a reaction-diffusion system and studies on this topic date back to [4]. Rigorous proof of existence of traveling wave solution in a reaction-diffusion system often leads to phase space analysis such as in [2]. Not only the high dimension but also the singularity represented in the cross diffusion makes any rigorous proof a daunting task. Nevertheless, the reduced system is amenable to phase plane analysis and the orbit representing the traveling wave solution can be identified (see appendix).

Instead of having a lumped proliferation term as in [7] which only tracks net proliferation, our model treats birth and death separately, making it possible to gauge the underlying total proliferation of cancer cells. This is valuable information for personalized treatment design since most chemotherapy and radiotherapy target proliferating cells. Moreover, the structural information is also potentially useful, e.g., it may help deciding drug dose so that the drug can perfuse through the width of the proliferating rim. Research along this line has been conducted using the PI model [8].

We recognize the fact that the cancer is constantly evolving over its course of growth and the observed cancer profile at two different times is not scale invariant. We understand that the parameters of the model may not stay constant over time. In this paper, we devise a method which uses two MR images taken at two consecutive times before surgery, and our method is feasible whether the two scans are consistent with invariant cancer profile or not. It is straightforward to extend the current method to make use of MR images taken at three or even more time points. By updating parameters as more data is acquired, we are essentially doing data assimilation. There has been research on applying full-fledged data assimilation to cancer modeling [9, 13]. Our method stands out being mathematically intuitive and computationally straightforward. In the case when only one pre-surgery MR scan is available, we present a way to estimate parameters involving natural and experimentally verifiable assumptions. The major contributions of this paper is presenting two novel ways of making use of scarce data which are routinely available in clinical settings. So we hope our method would find wide and practical applications compared to large-scale computational models [3, 16], which often focus on fitting experimental data sets that include many data points.

Acknowledgments

The authors would like to thank Leslie Baxter and Leland Ho at Barrow Neurological Institute for providing MR images. The work is supported by an grant from Arizona Biomedical Research Center.

References

1. J. Canosa, On a Nonlinear Diffusion Equation Describing Population Growth, *IBM Journal of Research and Development*, **17** (1973), 307–313, URL http://ieeexplore.ieee.org/document/5391351/.
2. S. Dunbar, Travelling wave solutions of diffusive Lotka-Volterra equations, *Journal of Mathematical Biology*, **17** (1983), 11–32, URL http://link.springer.com/10.1007/BF00276112.
3. S. E. Eikenberry, T. Sankar, M. C. Preul, E. J. Kostelich, C. J. Thalhauser and Y. Kuang, Virtual glioblastoma: Growth, migration and treatment in a three-dimensional mathematical model, *Cell Proliferation*, **42** (2009), 511–528.
4. R. A. Fisher, The wave of advance of advantageous genes, *Annals of Eugenics*, **7** (1937), 355–369, URL http://doi.wiley.com/10.1111/j.1469-1809.1937.tb02153.x.
5. P. Gerlee and S. Nelander, Travelling wave analysis of a mathematical model of glioblastoma growth, *Mathematical Biosciences*, **276** (2016), 75–81, URL https://www.sciencedirect.com/science/article/abs/pii/S0025556416000602?via{%}3Dihub.
6. K. Harley, P. van Heijster, R. Marangell, G. J. Pettet and M. Wechselberger, Existence of Traveling Wave Solutions for a Model of Tumor Invasion, *SIAM Journal on Applied Dynamical Systems*, **13** (2014), 366–396, URL http://epubs.siam.org/doi/10.1137/130923129.
7. P. R. Jackson, J. Juliano, A. Hawkins-Daarud, R. C. Rockne and K. R. Swanson, Patient-Specific Mathematical Neuro-Oncology: Using a Simple Proliferation and Invasion Tumor Model to Inform Clinical Practice, *Bulletin of Mathematical Biology*, **77** (2015), 846–856, URL http://link.springer.com/10.1007/s11538-015-0067-7.
8. M. Kim, J. Kotas, J. Rockhill, M. Phillips, M. Kim, J. Kotas, J. Rockhill and M. Phillips, A Feasibility Study of Personalized Prescription Schemes for Glioblastoma Patients Using a Proliferation and Invasion Glioma Model, *Cancers*, **9** (2017), 51, URL http://www.mdpi.com/2072-6694/9/5/51.
9. E. J. Kostelich, Y. Kuang, J. M. McDaniel, N. Z. Moore, N. L. Martirosyan and M. C. Preul, Accurate state estimation from uncertain data and models: an application of data assimilation to mathematical models of human brain tumors, *Biology Direct*, **6** (2011), 64, URL http://biologydirect.biomedcentral.com/articles/10.1186/1745-6150-6-64.
10. Y. Kuang, J. D. Nagy and S. E. Eikenberry, *Introduction to mathematical oncology*, Chapman and Hall/CRC.
11. A. Madzvamuse, R. Barreira and A. Gerisch, Cross-Diffusion in Reaction-Diffusion Models: Analysis, Numerics, and Applications, Springer, Cham, 2017, 385–392, URL http://link.springer.com/10.1007/978-3-319-63082-3{_}61.

12. N. L. Martirosyan, E. M. Rutter, W. L. Ramey, E. J. Kostelich, Y. Kuang and M. C. Preul, Mathematically modeling the biological properties of gliomas: A review, *Mathematical Biosciences and Engineering*, **12** (2015), 879–905, URL http://www.ncbi.nlm.nih.gov/pubmed/25974347http://www.aimsciences.org/journals/displayArticlesnew.jsp?paperID=11020.

13. J. McDaniel, E. Kostelich, Y. Kuang, J. Nagy, M. C. Preul, N. Z. Moore and N. L. Matirosyan, Data Assimilation in Brain Tumor Models, Springer, New York, NY, 2013, 233–262, URL http://link.springer.com/10.1007/978-1-4614-4178-6{_}9.

14. M. L. Neal, A. D. Trister, T. Cloke, R. Sodt, S. Ahn, A. L. Baldock, C. A. Bridge, A. Lai, T. F. Cloughesy, M. M. Mrugala, J. K. Rockhill, R. C. Rockne and K. R. Swanson, Discriminating Survival Outcomes in Patients with Glioblastoma Using a Simulation-Based, Patient-Specific Response Metric, *PLoS ONE*, **8** (2013), e51951, URL https://dx.plos.org/10.1371/journal.pone.0051951.

15. A. D. Norden and P. Y. Wen, Glioma therapy in adults, *The neurologist*, **12** (2006), 279–92, URL http://www.ncbi.nlm.nih.gov/pubmed/17122724.

16. E. M. Rutter, T. L. Stepien, B. J. Anderies, J. D. Plasencia, E. C. Woolf, A. C. Scheck, G. H. Turner, Q. Liu, D. Frakes, V. Kodibagkar, Y. Kuang, M. C. Preul and E. J. Kostelich, Mathematical Analysis of Glioma Growth in a Murine Model, *Scientific reports*, **7** (2017), 2508, URL http://www.ncbi.nlm.nih.gov/pubmed/28566701{%}5Cnhttp://www.pubmedcentral.nih.gov/articlerender.fcgi?artid=PMC5451439.

17. J. A. Sherratt, Wavefront propagation in a competition equation with a new motility term modelling contact inhibition between cell populations, *Proceedings of the Royal Society of London. Series A: Mathematical, Physical and Engineering Sciences*, **456** (2000), 2365–2386, URL http://www.royalsocietypublishing.org/doi/10.1098/rspa.2000.0616.

18. J. A. Sherratt and M. A. Chaplain, A new mathematical model for avascular tumour growth, *Journal of Mathematical Biology*, **43** (2001), 291–312, URL http://link.springer.com/10.1007/s002850100088.

19. T. L. Stepien, E. M. Rutter and Y. Kuang, A data-motivated density-dependent diffusion model of in vitro glioblastoma growth., *Mathematical biosciences and engineering : MBE*, **12** (2015), 1157–72, URL http://www.ncbi.nlm.nih.gov/pubmed/26775861.

20. T. L. Stepien, E. M. Rutter and Y. Kuang, Traveling Waves of a Go-or-Grow Model of Glioma Growth, *SIAM Journal on Applied Mathematics*, **78** (2018), 1778–1801, URL https://epubs.siam.org/doi/10.1137/17M1146257.

21. K. R. Swanson, R. C. Rockne, J. Claridge, M. A. Chaplain, E. C. Alvord and A. R. A. Anderson, Quantifying the Role of Angiogenesis in Malignant Progression of Gliomas: In Silico Modeling Integrates Imaging and Histology, *Cancer Research*, **71** (2011), 7366–7375, URL http://www.ncbi.nlm.nih.gov/pubmed/21900399http://www.pubmedcentral.nih.gov/articlerender.fcgi?artid=PMC3398690http://cancerres.aacrjournals.org/cgi/doi/10.1158/0008-5472.CAN-11-1399.

22. K. R. Swanson, R. C. Rostomily and E. C. Alvord, A mathematical modelling tool for predicting

survival of individual patients following resection of glioblastoma: a proof of principle, *British Journal of Cancer*, **98** (2008), 113–119, URL http://www.nature.com/articles/6604125.

Supplementary

We perform phase plane (w-p plane, see Figure 1) analysis of (2.7) to show the existence of a trajectory that starts from $(1,0)$ and ends at $(w^*,0)$ where $w^* \geq 0$ if (2.2) are satisfied. The Jacobian matrix at (1,0) is

$$\begin{bmatrix} 0 & -\hat{\rho} \\ 0 & \hat{\rho} \end{bmatrix}. \tag{4.1}$$

It follows that $(1,0)$ is an unstable fixed point and the trajectory starting here has slope -1 which is the direction of the unstable manifold. We also note that

$$\frac{d^2p}{dw^2} = \frac{\delta'(w)g(w) - \delta(w)g'(w)}{\hat{\rho}g(w)^2} < 0 \tag{4.2}$$

for $w \in (0,1)$ because of the assumptions (2.2) we proposed on $g(w)$ and $\delta(w)$. (4.2) ensures that the trajectory must remain below the line $p = 1-w$ and that there is no periodic solutions. Moreover, since $\frac{dw}{dz}|_{w=0} = 0$, the trajectory cannot cross p-axis. Assuming $g(w)$ and $\delta(w)$ are continuous, there must be a $w^\dagger \in (0,1)$ such that $\rho g(w^\dagger) = \delta(w^\dagger)$. For $w > w^\dagger$, the trajectory has positive slope and hence heading down to the w-axis. Thus it must intersect the w-axis at some point $w^* \in (0, w^\dagger)$.

AIMS Press